JOURNAL OF CATALYSIS 60, 441–451 (1979)

Thermal Desorption Study of the Acetic Acid Decomposition on Clean Ni/Cu(110) Alloy Surfaces

DAVID H. S. YING AND ROBERT J. MADIX

Department of Chemical Engineering, Stanford University, Stanford, California 94305

Received July 20, 1978; revised June 1, 1979

The decomposition of acetic acid was studied on a clean Ni/Cu(110) alloy single crystal by means of thermal desorption spectroscopy. The primary alloy surface composition employed in this work was 37% Ni and 63% Cu as measured by Auger electron spectroscopy. Acetate was the predominant surface intermediate observed, giving rise to the CO_2 and H_2 decomposition products observed, in analogous fashion to the decomposition of formic acid. Surface carbon residue was also detected and could be driven into the bulk by annealing the sample above 900°K. The rate constant for the decomposition of the acetate intermediate on the alloy was found to be $10^{13.5}\exp(-33(\text{kcal/mol})/RT)\text{sec}^{-1}$. The autocatalytic decomposition of both carboxylic acids previously observed on a clean Ni(110) surface was totally suppressed. The product distribution from acetic acid observed on both the 37% Ni/65% Cu alloy and the carburized Ni(110) surfaces were very similar, indicating chemical similarities between these two surfaces. At high coverages of the acetate intermediate the activation energy for CO_2 formation increased by 14 kcal/gmol. This effect was attributed to strong attractive interactions in the adsorbate layer.

INTRODUCTION

Metal alloys have long been a subject of interest in catalysis (*1–7*). Work with Cu/Ni alloys has clearly indicated the importance of the Cu/Ni surface composition in determining the selectivity for a variety of reactions (*1*, *2*, *4*, *10*). Recent photoemission work on the Ni/Cu alloy system by Spicer *et al.* (*8*, *9*), utilizing short electron escape depths, illustrated that the surface electronic properties of the alloy were simply the superposition of the surface electronic property of each separate metal. The decomposition of the simplest carboxylic acid (formic acid) on a clean, (110)-oriented Ni/Cu alloy single crystal (*10*) has shown that the product selectivity ratio is strongly governed by the surface composition of the alloy. The selectivity was controlled by the degree of admixture of two different reaction pathways involving adsorbed formic anhydride or formate, respectively. Whereas on Ni(110) the flash decomposition of formic acid proceeded solely via the anhydride intermediate (*11–13*), on Cu(110) the intermediate was formed alone (*14*). Both dehydration and dehydrogenation pathways were observed on the Ni/Cu alloy. The CO/CO_2 product ratio decreased with increasing copper surface concentration. The decomposition of acetic acid on pure Ni(110) surface was investigated by Madix *et al.* (*15*), and an autocatalytic reaction similar to that of formic acid decomposition was observed. The surface intermediate was identified as acetic anhydride. It was interesting to see whether

0021-9517/79/150441-11$02.00/0

this autocatalytic decomposition of acetic acid was suppressed by the presence of copper as for the formic acid decomposition, and whether a similarity existed in the surface intermediates from the decomposition of both carboxylic acids on the alloy surface. The primary goal of the present work was to study the decomposition of acetic acid on clean Ni/Cu(110) alloy single crystals and to see to what extent the chemical analogy for the reactivity of the carboxylic acids would persist on the alloy surface.

Chemical similarities between nickel carbide surface and the Ni/Cu alloy with low nickel surface concentration (37%) were evident from the comparison of the formic acid decomposition on both the carburized Ni(110) surface (*16–18*) and the alloy surface (*10*). Adsorbed formate ($HCOO_{(a)}$) was the predominant surface intermediate observed on both of these surfaces, and the nearly identical CO/CO_2 product ratio strongly suggested the chemical similarity between these two surfaces. Preliminary results of the acetic acid decomposition on a carburized Ni(110) surface (*19*) indicated that acetate was the predominant surface intermediate, giving rise to the CO_2, H_2, and absorbed carbon observed. The present study provided a further test of the suggestion of the chemical similarities between the nickel carbide and the Ni/Cu alloy surfaces.

EXPERIMENTAL

Temperature-programmed reaction spectroscopy was employed to study the decomposition of acetic acid on a clean Ni/Cu(110) alloy single crystal. The clean alloy surface was achieved by ion bombardment and subsequent annealing at a higher temperature, following by quickly cooling back to room temperature. The surface composition of the alloy was measured by Auger electron spectroscopy (AES). The quantitative determination of the alloy surface composition by AES was described previously (*10*, *20–22*). The $M_1M_{4,5}M_{4,5}$ Auger transition spectrum near 100 eV was doubly integrated to obtain the surface composition.

When a clean alloy surface was obtained, the previously purified acetic acid vapor (*15*) was dosed onto the sample surface in the ultrahigh vacuum reaction chamber. The ambient pressure was maintained in the 10^{-10} Torr region by means of an ion pump and a titanium sublimation pump. The detailed arrangement of the equipment was described previously (*10*, *23*). The sample temperature during adsorption was controlled by a liquid nitrogen cooling tube compensated by partial heating of the sample from a tungsten filament. After dosing, the sample was flashed linearly with time, and the partial pressure rise of each product gas was recorded by UTI quadrupole mass spectrometer as a function of the sample temperature. The mass spectrometric signal was directly proportional to the desorption rate due to the high pumping speed of the system. There was an appreciable amount of surface carbon residue detected by Auger electron spectroscopy after each flash. This surface carbon residue could be driven into the bulk by annealing the sample at 900°K, thereby regenerating a clean alloy surface. However, this method could be applied *solely* to the 37% Ni/63% Cu alloy surface, because the other higher nickel surface concentration alloys were achieved by annealing at a lower temperature, which was not sufficient to drive all the surface carbon into the bulk. Hence, surfaces of all other compositions were regenerated by sputtering and annealing at the required temperatures after each flash.

A shorthand notation was employed to identify the origin of the desorbing gas as follows:

$$X(\gamma)/Y$$

where X was the desorbing gas observed
(γ) was the binding state of the gas
Y was the preadsorbed gas.

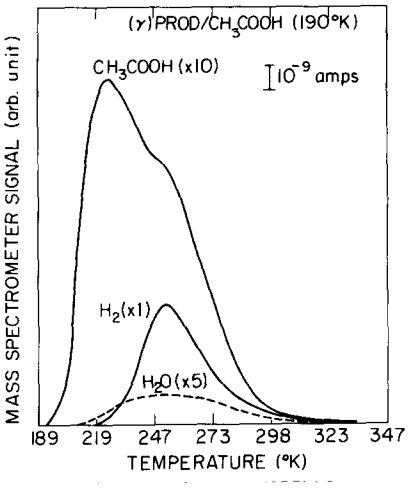

FIG. 1. Product distribution in the low-temperature region following and adsorption of CH_3COOH on an alloy with a surface composition of 37% Ni and 63% Cu at 190°K. Heating rate was 18°K sec^{-1}. Saturation exposure.

For example,

$$H_2(\gamma)/CH_3COOH$$

refers to the γ state of the H_2 product following the adsorption of CH_3COOH.

RESULTS

Figures 1 and 2 show the product distribution in two temperature regions following the adsorption of CH_3COOH at 190°K on an alloy with a surface composition of 37% Ni and 63% Cu. CO_2 and H_2 were the major decomposition products observed. The hydrogen product desorption spectrum exhibited two distinct peaks at 253 and 543°K labeled as $H_2(\gamma)$ and $H_2(\beta)$, respectively, as shown in Figs. 1 and 2. The $H_2(\beta)/H_2(\gamma)$ product ratio was 2.7 $\pm$ 0.2. A comparison of the $H_2(\gamma)$ product peak with the H_2/H_2 desorption spectrum (*14*) indicated that the $H_2(\gamma)$ product was desorption limited. The $H_2(\beta)$ spectrum had a shoulder at around 500°K, indicating that this peak was a composite. The CO_2 and $H_2(\beta)$ desorption spectra showed nearly identical shape and peak position, suggesting that these products were evolved from the same rate-limiting steps. The small amount of CO product, after subtracting out the cracking fraction of the CO_2 product at mass 28, showed a broad peak; the peak position could not be located exactly. This CO product only amounted to less than one-tenth of the CO_2 product. In addition, small amounts of CH_3COOH and H_2O were detected in both the low- and the high-temperature regions. The $CH_3COOH(\gamma)$ peak corresponds to the desorption of the parent molecule intact from the alloy surface. The pumping speeds of both the H_2O and CH_3COOH were not known, so it was impossible to make quantitative estimates of the H_2O and CH_3COOH formed. However, the mass spectrometric signals of the $H_2O(\beta)$ and $CH_3COOH(\beta)$ (see Fig. 2) peaks were less than 1% of the CO_2 product, indicating they were insignificant amounts with respect to the total amount of products formed.

When the adsorption temperature was

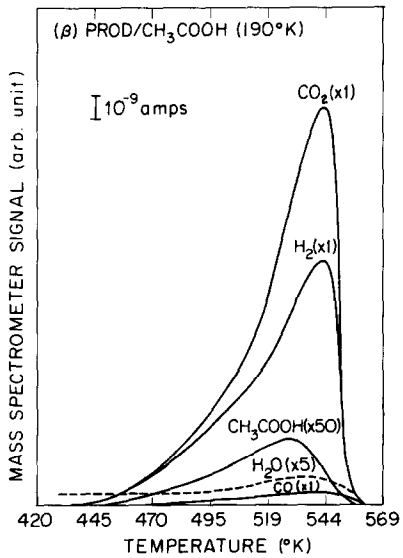

FIG. 2. Product distribution in the high-temperature region following the adsorption of CH_3COOH on an alloy with a surface composition of 37% Ni and 63% Cu at 190°K. Heating rate was 18°K sec^{-1}. Saturation exposure.

increased from 190 to 298°K, CO_2 and H_2 were still the major products observed as shown in Fig. 3. Small amounts of CO, H_2O, and CH_3COOH were also detected. Since the low-temperature γ states were not observed in the room temperature study, the β state symbol was deleted in the following discussion. Although the same decomposition products were observed when the adsorption temperature was increased from 190 to 298°K, the peak position shifted to a lower temperature, and the total amount of product was reduced by about 35%, indicating a reduction in sticking probability of CH_3COOH.

Figures 4 and 5 show the desorption of the CO_2 product at saturation exposure of acetic acid as a function of adsorption temperature. The results are summarized in Table 1. The CO_2 peak position shifted continuously to lower temperatures as the adsorption temperature was increased until at 457°K the peak moved back to a slightly higher temperature. This abrupt reversal in the shift of the CO_2 peak position at the adsorption temperature of 457°K occurred because the adsorption temperature was sufficiently high to prevent the formation of the CO_2 product from the lower temperature states. In addition to the shift of the peak position and the attenuation of the

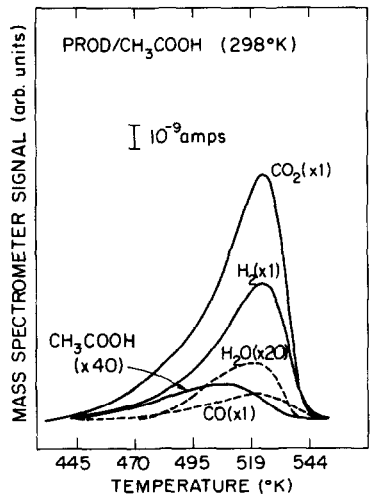

FIG. 3. Product distribution following the adsorption of CH_3COOH on an alloy with a surface composition of 37% Ni and 63% Cu at 298°K. Heating rate was 18°K sec^{-1}. Saturation exposure.

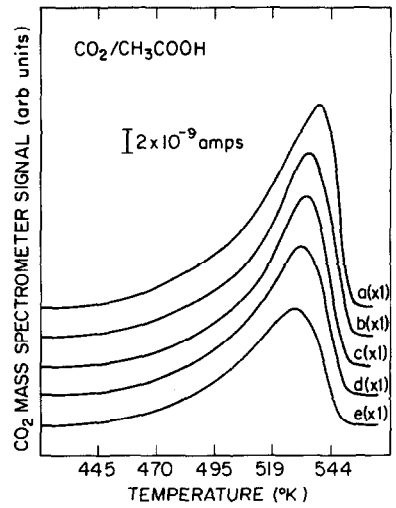

FIG. 4. CO_2 product desorption spectra as a function of adsorption temperature on a 37% Ni/63% Cu alloy surface. (a) Adsorbed at 190°K; (b) adsorbed at 219°K; (c) adsorbed at 247°K; (d) adsorbed at 273°K; (e) adsorbed at 298°K. Saturation exposure of CH_3COOH. Heating rate was 18°K sec^{-1}.

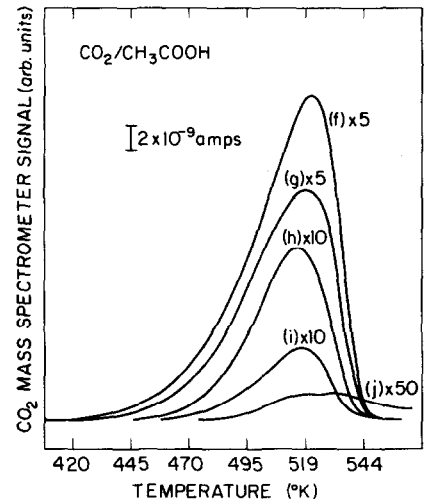

FIG. 5. CO_2 product desorption spectra as a function of adsorption temperature on a 37% Ni/63% Cu alloy surface. (f) Adsorbed at 347°K; (g) adsorbed at 395°K; (h) adsorbed at 445°K; (i) adsorbed at 457°K. Saturation exposure of CH_3COOH. Heating rate was 18°K sec^{-1}. (j) Adsorbed at 470°K.

TABLE 1

CO_2 Peak Position as a Function of the Adsorption Temperature

Adsorption temperature (°K)	Peak position (°K)
190	540.0
219	535.2
247	534.0
273	531.5
298	527.7
347	522.0
395	519.0
445	515.0
457	517.0

product formed, the profile of the CO_2 changed as the adsorption temperature was varied. Table 2 shows the ratio of the integrated area in front of and behind the peak maximum (A_i/A_b) for all the CO_2 spectra shown in Figs. 4 and 5. This ratio varied from 3.8 to 1.7. For a first-order process, theoretical calculation indicates a ratio of 1.72, suggesting that the CO_2 desorption following the adsorption of the parent molecule at 445°K is a first-order process.

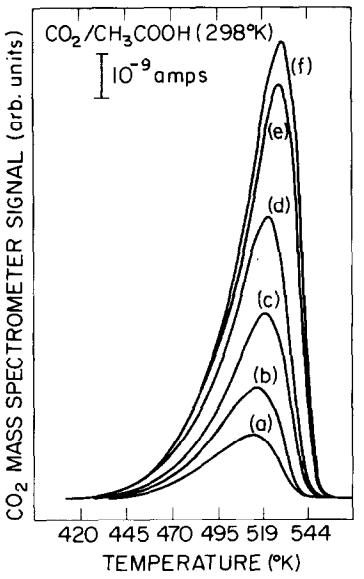

FIG. 6. Coverage variation study of the CO_2 product following the adsorption of the acetic acid at room temperature on a 37% Ni 63% Cu alloy surface. Relative exposures are pressure in the dosing volume times the exposure time. Heating rate was 18°K sec^{-1}. (a) 250 μS; (b) 500 μS; (c) 1250 μS; (d) 3750 μS; (e) 10000 μS; (f) 15000 μS.

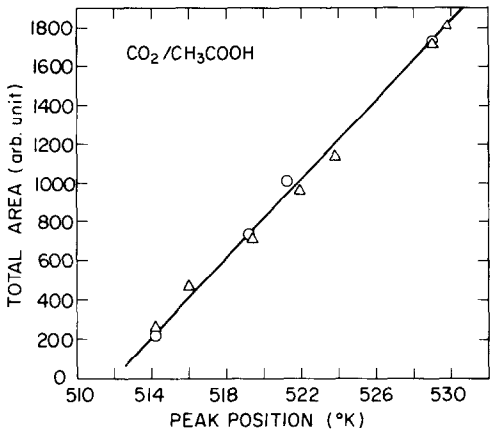

FIG. 7. A plot of the CO_2 product versus its peak position for the variation of adsorption temperature and coverage studies. Heating rate was 18°K sec^{-1}.

The effect of varying the acetic acid exposure was also investigated. Figure 6 shows the CO_2 product spectra as a function of the coverage following the adsorption of the parent molecule at room temperature on the 37% Ni surface. When the coverage was decreased, the CO_2 peak position also shifted to lower temperatures, suggesting that the shift of the CO_2 peak position

TABLE 2

Variation of Adsorption Temperature Study

Adsorption temperature (°K)	A_i/A_b[a]
190	3.8 ± 0.2
219	2.5 ± 0.2
247	2.7 ± 0.2
273	2.9 ± 0.2
298	3.0 ± 0.2
347	2.3 ± 0.2
395	2.3 ± 0.2
445	1.7 ± 0.2

[a] A_i is the integrated area in front of the peak maximum; A_b is the integrated area behind the peak maximum.

with adsorption temperature was simply a coverage variation effect. Figure 7 shows a plot of the amount of CO_2 product formed versus its peak position observed with both the variation of adsorption temperatures and coverage. The data points from both studies agreed excellently, supporting the above suggestion of the variation of the adsorption temperature to be a coverage effect.

An isothermal analysis (*25*) was employed in an attempt to measure the reaction order of the CO_2 peak. Figure 8 shows a ln–ln plot of the CO_2 desorption rate versus the coverage. At low coverages the reaction order approached unity, but with increasing coverage the apparent order decreased. This behavior was consistent with an activation energy which increased with coverage, in agreement with the spectra of Figs. 4–6.

The activation energy for the CO_2 formation was measured by means of a heating rate variation method. The details of this method were described elsewhere (*26*). Figure 9 shows the plot of $\ln(\beta/T_p^2)$ versus $1/T_p$ for the CO_2 peak at saturation coverage. The activation energy was found to be 47 kcal/mol. With an assumption of a pseudo-first-order process, the preexponential factor was estimated to be $10^{19.7}$ sec^{-1}. Since the CO_2 peak shifted to a

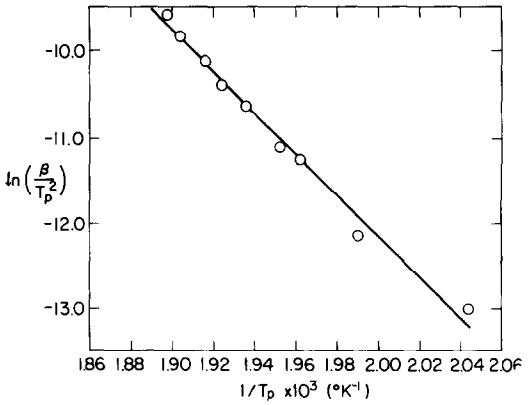

FIG. 9. Activation energy of the CO_2 product formation determined by a heating rate variation method. Saturation exposure of CH_3COOH at room temperature.

lower temperature at a lower coverage, the same heating rate variation method was applied to measure the activation energy for the CO_2 peak at a low CH_3COOH exposure. The data were quite scattered due to the difficulty in controlling the low acetic acid exposure and the sensitivity of the CO_2 peak position to coverage. However, since low coverage CO_2 spectra were obtainable by adsorbing at higher temperatures, the activation energy for the CO_2 formation at low coverage was measured by applying the heating rate variation method to the CO_2 peak obtained at saturation coverage following the adsorp-

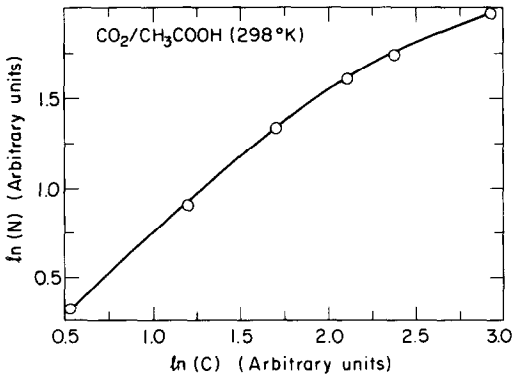

FIG. 8. Isothermal plot. Plotting the logarithm of the CO_2 desorption rate versus the coverage following the adsorption of acetic acid on a 37% Ni/63% Cu alloy surface at room temperature.

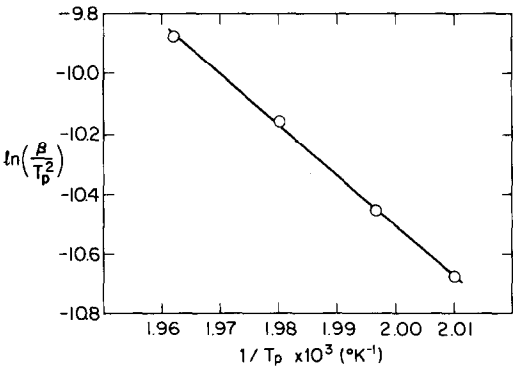

FIG. 10. Activation energy of the CO_2 product formation determined by a heating rate variation method. Saturation exposure of CH_3COOH at 457°K.

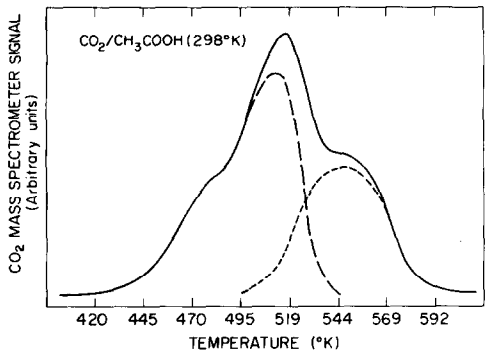

FIG. 11. CO_2 product desorption spectrum observed on a 37% Ni/63% Cu alloy with surface carbon contaminant. ——— Experimental spectrum with surface carbon contaminant. — — Experimental spectrum from a *clean* alloy surface. — — — The difference between ——— and — —.

tion of the parent molecule at 456°K, as shown in Fig. 10. The activation energy was found to be 33 kcal/mol, and the preexponential factor was estimated to be $10^{13.5}$ sec^{-1} with the assumption of a first-order process.

In addition to the decomposition products observed, surface carbon was detected by Auger electron spectroscopy after a few flashes, the presence of the surface carbon caused a high temperature shoulder to appear in the CO_2 spectrum and shifted the peak position slightly to a higher temperature. After subtracting off the contribution due to the *clean* alloy surface, an extra CO_2 peak was obtained as shown in Fig. 11. The peak position of this additional CO_2 peak matched that observed from the decomposition of acetic acid on a carburized Ni(110) surface (*19*), suggesting that this extra CO_2 peak was due to the carburized nickel sites on the alloy surface. By annealing the sample to 900°K, a *clean* alloy surface was regenerated, and the *normal* CO_2 peak observed on a clean alloy surface was reproduced.

DISCUSSION

Acetic acid decomposed on the 37% Ni/63% Cu alloy surface forming primarily CO_2, H_2, and surface carbon. The reaction mechanism proposed was as follows:

$$CH_3COOH_{(g)} \rightarrow CH_3COO_{(a)} + H_{(a)} \quad (A)$$

$$CH_3COOH_{(g)} \rightarrow CH_3COOH_{(a)} \quad (B)$$

$$CH_3COOH_{(a)} \rightarrow CH_3COOH_{(g)} \quad (C)$$

$$2H_{(a)} \rightarrow H_{2(g)} \quad (D)$$

$$CH_3COO_{(a)} \rightarrow CO_{2(g)} + 3H_{(a)} + C \quad (E)$$

$$2H_{(a)} \rightarrow H_{2(g)} \quad (F)$$

$$CH_3COO_{(a)} + H_{(a)} \rightarrow CH_3COOH_{(g)} \quad (G)$$

The first step was the dissociative adsorption of the parent molecule forming the acetate surface intermediate ($CH_3COO_{(a)}$). This dissociative adsorption was inferred from the presence of two widely separated hydrogen peaks: $H_2(\beta)$ and $H_2(\gamma)$. In addition, the $H_2(\beta)/H_2(\gamma)$ ratio was close to three which was a correct stoichiometric ratio between the oxygen-bonded hydrogen and the carbon-bonded hydrogen atoms; this $H_2(\beta)/H_2(\gamma)$ ratio was analogous to the 1:1 ratio for $D_2/DCOOH$:$H_2/DCOOH$ observed in the decomposition of formic acid on the same alloy surface (*10*), forming the formate intermediate. Furthermore the dominant CO_2 product also indicated the existence of the acetate surface intermediate.

Step (E) represented the decomposition of the acetate to form carbon dioxide, adsorbed hydrogen atoms, and surface carbon residue. Since no CO_2 binding state existed on the alloy surface, the CO_2 product desorbed immediately upon its formation. Hence the rate of CO_2 formation was decomposition limited. The recombination of the hydrogen atoms shown in step (F) was a fast process in this high-temperature region, leaving the decomposition of the acetate to be the rate governing step. Therefore, the CO_2 and the $H_2(\beta)$ products exhibited identical desorption spectra. The surface carbon residue could be driven into the bulk by flashing the sample to the

initial annealing temperature (900°K) at each flash, so that a clean alloy surface was ready for the subsequent flash. In addition, once when the acetate ($CH_3COO_{(a)}$) started to decompose, the hydrogen atoms captured some of the acetate intermediates before they decomposed to form the acetic acid molecule which desorbed from the surface to give rise to the trace of CH_3COOH product observed. This capture of the acetate intermediate was analogous to that of the $CH_3O_{(a)}$ intermediate observed in the oxidation of methanol on Cu(110) and Ag(110) surfaces (*27*).

With an assumption of a linear coverage-dependent activation energy, one could qualitatively explain the data shown in Fig. 8. The calculated activation energy change from low coverage to saturation was 1.8 ± 0.2. Equation (1),

$$N = \theta\nu_1 \exp(-E/RT) \qquad (1)$$

is a first-order rate expression. N is the normalized reaction rate, θ is the fractional coverage ($0 \leq \theta \leq 1$), ν_1 is the first order preexponential function, E is the activation energy, and T is the absolute temperature. If the activation energy was assumed to increase linearly with coverage as shown below

$$E = E_0 + \alpha\theta \qquad (2)$$

where α is a *positive* constant, Eq. (1) can be written as follows:

$$N = \theta\nu_1 \exp(-(E_0 + \alpha\theta)/RT). \qquad (3)$$

By taking the logarithm of Eq. (3), one obtains the expression.

$$\ln(N) = \ln(\theta) - \alpha\theta/RT + \ln(\nu_1) - E_0/RT. \qquad (4)$$

Equation (4) can be arranged to obtain

$$\theta = (RT/\alpha)\ln(\theta/N) + (\ln(\nu_1) - E_0/RT). \qquad (5)$$

Therefore, a plot of θ as a function of $\ln(\theta/N)$ would give an estimate of the α value. Figure 12 shows a plot of θ versus $\ln(\theta/R)$ for the CO_2 peak at isothermal condition; a fairly reasonable straight line was obtained. The value of α was calculated to be 1.8 ± 0.2 kcal/mol. Figure 13 shows the fit of the CO_2 spectrum observed in the high adsorption temperature study. The gross feature of the CO_2 peak was fitted by the theoretically simulated spectrum. A precise fitting was not obtained as normally expected when a composite peak was fitted by a pseudo-single process.

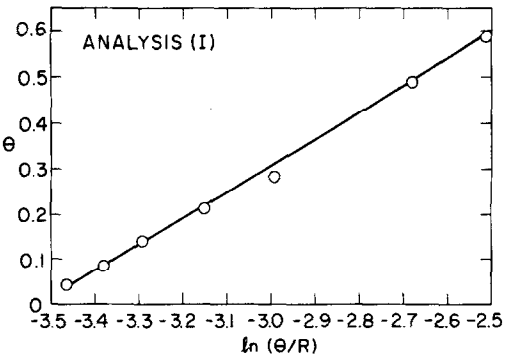

FIG. 12. A plot of θ versus $\ln(\theta/R)$ for the CO_2 peak at isothermal conditions.

It is important to note that this value of α was used merely as a fitting parameter however. The values of A_i/A_b in Table 1 clearly show that at high coverages the CO_2 peak is a composite peak, as values of 1.7 would be expected for a simple first-order

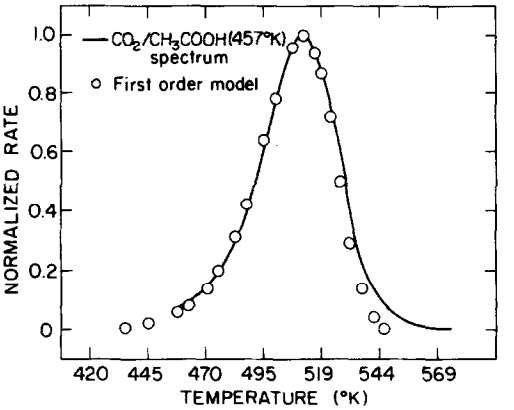

FIG. 13. Theoretical simulation to fit the CO_2 product spectrum following a saturation exposure of CH_3COOH at 457°K. First-order process activation energy was 33 kcal/mol. Preexponential factor was $10^{13.5}$ sec^{-1}. Heating rate was 13°K sec^{-1}.

desorption step. This value was observed only for the highest adsorption temperatures (lowest initial coverages). The high values of A_i/A_b indicate a major reaction peak to the left of the peak maximum and this contribution is easily observed in Figs. 2 and 3, for example. Another indication that the high coverage peaks are a composite is the high apparent activation energy and preexponential factors obtained from the heating rate variation (Fig. 9). Nonetheless, the low coverage data do provide an accurate measure of the decomposition rate constant for the acetate intermediate.

Qualitatively, the Ni/Cu alloy interacts similarly with both formic acid and acetic acid. Both carboxylic acids were observed to decompose autocatalytically on the clean Ni(110) surface (*11–13*, *15*). This autocatalytic decomposition was attributed to island formation of the formic anhydride and acetic anhydride intermediates due to attractive interactions. The presence of copper on the Ni/Cu alloy surface totally suppressed both autocatalytic reactions. The study of the decomposition of formic acid on Ni/Cu alloy surfaces (*10*) indicated an increasing CO to CO_2 product selectivity ratio as the alloy surface was enriched with nickel atoms. Although the decomposition of acetic acid was not studied in detail on surfaces of higher nickel concentrations, preliminary results indicated that the CO to CO_2 product ratio increased with increasing nickel surface concentration, following the same trend as observed in the formic acid decomposition. Furthermore, analogous to the formate ($HCOO_{(a)}$) intermediate predominant on the 37% Ni–63% Cu alloy surface, acetate ($CH_3COO_{(a)}$) was the dominant intermediate on the alloy surface of the same composition. It is interesting to note that the ratio of the limiting preexponential factor for $HCOO_{(a)}$ (*10*) and the preexponential factor estimated with the assumption of a first-order process for $CH_3COO_{(a)}$ was approximately 3.0. This estimated ratio was close to the square root of the inverse ratio of the masses for the H- and CH_3-groups (3.9). If the vibration of the H–COO and CH_3–COO bonds was involved in their transition states to give rise of their products, the ratio of their vibrational frequency should follow the square root of the inverse ratio of their masses (H- and CH_3-groups). Hence the estimated preexponential factor ratio suggests that the motions of these hydrogen and methyl groups were involved in the decomposition steps. It should be pointed out that the assumption of a first-order process might overestimate the preexponential factor for $CH_3COO_{(a)}$. If it was assumed that the acetic anhydride intermediate was absorbed on the surface nickel sites of the alloy and was responsible for the slight amount of CO product observed (in analogy to the formic anhydride in the decomposition of formic acid on the same alloy surface (*10*) the high preexponential factor for acetic anhydride decomposition (*15*) would cause an apparently larger preexponential factor for acetate decomposition. Fortunately, the CO product was so small that the correction due to the presumed acetic anhydride would not be substantial. In any event, the correction would increase the preexponential factor ratio, approaching the value of 3.9.

The methyl fragment which was detached from the acetate intermediate behaved somewhat differently from the hydrogen atom detached from the formate intermediate. The hydrogen atom recombined immediately with another hydrogen atom to form H_2 which desorbed from the surface, whereas the methyl species further decomposed to form adsorbed hydrogen and carbon residue, with the adsorbed hydrogen atoms recombining to produce H_2. It was attempted, though unsuccessfully, to stabilize and capture the methyl group with background hydrogen gas to

form methane. This surface readily adsorbed hydrogen, and some recombination to form CH_4 would be expected if CH_3 were relatively long-lived. No methane was observed. This failure to capture the methyl group indicated that the methyl fragment is not a stable species residing on the alloy surface.

It has been suggested that the presence of surface carbidic carbon modifies the surface reactivity of nickel in a fashion similar to alloying with a group IB element (*10*). This argument was partially based upon the comparison of the adsorption and desorption of H_2 and CO on Ni/Cu(110) and on Ni(100)(2 × 1)C. Practically, the carbide surface does not chemisorb hydrogen (*28*). Hydrogen desorption state was observed on Ni/Cu alloy surface (*24*), but this adsorption was solely due to pure surface nickel binding sites. No H_2 desorption state which can be associated with pure copper or mixed copper–nickel binding sites was detected. The presence of surface carbidic carbon reduces the CO binding energy on pure nickel sites from 32 to 21 kcal/mole (*17*, *28*), lowering the CO desorption peak temperature by about 80°C. The CO desorption spectrum on Ni/Cu alloy surface (*9*, *10*, *24*) showed multiple peaks which retained the impurities of the pure nickel and pure copper binding sites and which included a mixed Ni–Cu binding or "alloy" sites. The carburized nickel binding site for CO showed a bind energy between the pure nickel and mixed Ni–Cu binding states, lying closer to the mixed state and supporting the qualitative similarity between the alloy and carbide surfaces.

Another similarity was found in the close resemblance between the decomposition of formic acid on both surfaces. The formic acid molecule dissociatively adsorbed on the carburized Ni(110) surface (*17*) to form a formate ($HCOO_{(a)}$) fragment, which decomposed to give rise of the hydrogen and carbon dioxide products. A slight amount of dehydration was also detected to form CO, amounting to approximately one-tenth of the CO_2 product. The dehydration to dehydrogenation selectivity ratio on the Ni/Cu alloy surface highly depends on the surface nickel concentration. This selectivity ratio increases with increasing nickel surface sites. On a 37% Ni–63% Cu surface (*10*), formate ($HCOO_{(a)}$) was identified as the major surface intermediate giving rise to the decomposition products which closely resembled those observed on the carburized nickel surface, strongly indicative of similar chemical reactivity between these two surfaces. Comparison of the acetic acid decomposition on these two surfaces further supports this indication, since the acetic acid decomposed on the carburized nickel and the alloy surface to form primarily CO_2 and H_2 products (*19*) via the acetate surface intermediate. The CO_2 and H_2 product spectra showed nearly identical peak temperature at 550°K.

SUMMARY

Acetate was the predominant surface intermediate observed in the acetic acid decomposition on an alloy with a surface composition of 37% Ni and 63% Cu. CO_2, H_2, and surface carbon were the major decomposition products observed. The activation energy for the decomposition of the acetate intermediate on the alloy was measured to be 33 kcal/mol. In addition, the decomposition energies for the acetate intermediates at low and high coverages differed by an amount of 14 kcal/mol, suggesting the formation of complex bonds at high coverage. The surface carbon residue carburized the surface nickel sites, giving rise of an additional CO_2 product peak matching that observed in the decomposition of acetic acid on a carburized Ni(110) surface. By annealing the sample to 900°K after each flash, the surface carbon residue diffused into the bulk, regaining a clean alloy surface.

Acetate was also the predominant surface intermediate observed on the carburized Ni(110) surface, supporting the suggestion that nickel carbide surface may chemically act like a Ni/Cu alloy.

ACKNOWLEDGMENTS

The authors wish to acknowledge support of this work by the National Science Foundation grant number NSF-DMR-74-22230-A01 through the Solid State Electronics Laboratories, Stanford Electronics Laboratories, Stanford University. Professor Madix would also like to express his gratitude to the Humboldt Foundation for support during the preparation of this manuscript.

REFERENCES

1. Verbeck, H., and Sachtler, W. M. H., *J. Catal.* **42**, 257 (1976).
2. Ponec, V., *Catal. Rev. Sci. Eng.* **11**(1), 1 (1975).
3. Ponec, V., and Sachtler, W. M. H., Proceedings of the 5th International Congress on Catalysis, Miami Beach, 1972, North Holland, Amsterdam, 1973, p. 645, paper No. 43.
4. Sinfelt, J. H., Carter, J. L., and Yates, D. J. C., *J. Catal.* **24**, 283 (1972).
5. Campbell, J. S., and Emmett, P. H., *J. Catal.* **7**, 252 (1967).
6. Dowden, D. A., and Reynolds, P. W., *Faraday Discuss. Chem. Soc.* **8**, 184 (1950).
7. Reynolds, P. W., *J. Chem. Soc.* 265 (1950).
8. Yu, K. Y., Ph.D. dissertation, Stanford University (1976).
9. Yu, K. Y., Helms, C. R., and Spicer, W. E., *Solid State Commun.* **18**, 1365 (1976).
10. Ying, D. H. S., and Madix, R. J., *J. Inorg. Chem.* **17**, 1103 (1978).
11. Falconer, J., and Madix, R. J., *Surface Sci.* **46**, 473 (1974).
12. Falconer, J., McCarty, J., and Madix, R. J., *Surface Sci.* **42**, 329 (1974).
13. Falconer, J., Ph.D. dissertation, Stanford University (1974).
14. Ying, D. H. S., and Madix, R. J., *J. Catal.*, in press.
15. Madix, R. J., Falconer, J., and Susko, A. M., *Surface Sci.* **54**, 6 (1976).
16. McCarty, J., Falconer, J., and Madix, R. J., *J. Catal.* **31**, 316 (1973).
17. McCarty, J., and Madix, R. J., *J. Catal.* **38**, 402 (1975).
18. McCarty, J., Ph.D. dissertation, Stanford University (1974).
19. Ying, D. H. S., and Madix, R. J., unpublished data.
20. Helms, C. R., *J. Catal.* **35**, 114 (1975).
21. Helms, C. R., and Yu, K. Y., *J. Vac. Sci. Technol.* **12**, 276 (1975).
22. Helms, C. R., Yu, K. Y., and Spicer, W. E., *Surface Sci.* **52**, 217 (1975).
23. McCarty, J., Falconer, J., and Madix, R. J., *J. Catal.* **30**, 235 (1973).
24. Yu, K. Y., Ling, D. T., and Spicer, W. E., *J. Catal.* **44**, 373 (1976).
25. Falconer, J., and Madix, R. J., *J. Catal.* **48**, 262 (1977).
26. Falconer, J., and Madix, R. J., *Surface Sci.* **48**, 393 (1975).
27. Wachs, I. E., and Madix, R. J., *Appl. Surface Sci.* **1**, 303 (1978).
28. McCarty, J., and Madix, R. J., *Surface Sci.* **54**, 121 (1976).